

HIGH ENERGY PHOTON EMISSION IN THE EARLY AFTERGLOW OF GRB'S

Asaf Pe'er^{1,2} and Eli Waxman¹

Draft version March 20, 2022

ABSTRACT

We consider the emission within the reball model framework of very high energy, > 1 GeV to > 1 TeV photons, on a minute time scale, during the onset of reball deceleration due to interaction with surrounding medium. Our time dependent numerical model includes exact treatment of electron synchrotron emission, inverse-Compton scattering, pair production, and evolution of electromagnetic cascades (initiated by pair production or photo-production of pions). We find that (i) The 1 GeV { 10 GeV flux is not sensitive to model parameters and is $\sim 10^{-7}$ erg cm⁻² sec⁻¹ for $z = 1$ bursts, well within the detection capabilities of GLAST; (ii) The sub-TeV flux depends on the surrounding medium density and on the fraction of thermal energy carried by the magnetic field, B : It ranges from $\sim 10^{-7}$ erg cm⁻² sec⁻¹ in the case of typical ISM density and $B \sim 10^{-4}$ to 10^{-10} erg cm⁻² sec⁻¹ in the case of a source surrounded by a wind and $B \sim 10^{0.5}$; (iii) The sub-TeV flux is detectable by high energy γ -ray experiments such as HESS, MAGIC, MILAGRO, and VERITAS; (iv) Combined 1 keV, 1 GeV and sub-TeV observations will allow to determine both B and the ambient medium density; (v) The spectra depend only weakly on the spectral index of the energy distribution of the accelerated electrons. Pion production energy loss of high energy protons may contribute significantly in the wind case to the luminosity of high energy photons. However, it is difficult to distinguish in this case between the electron and proton contributions since the spectral shape is determined primarily by the energy dependence of the pair production optical depth.

Subject headings: gamma rays: bursts | gamma rays: theory | radiation mechanisms: nonthermal

1. INTRODUCTION

In the standard reball model of gamma-ray-bursts (GRB's), the observable effects are due to the dissipation of kinetic energy in a highly relativistic reball (for reviews, see, e.g., Piran 2000; Meszaros 2002; Waxman 2003). The observed radiation is well explained as synchrotron and inverse-Compton emission from shock accelerated electrons. Electrons accelerated in internal shock waves within the expanding reball produce the prompt γ -ray emission, while electrons accelerated in the external shock wave driven by the reball into the surrounding medium produce the afterglow emission, from the X to the radio bands, that can last months after the burst (Paczynski & Rhoads 1993; Meszaros & Rees 1997; Vietri 1997a; Waxman 1997a; Waxman 1997b; Sari, Piran & Narayan 1998; Gruzinov & Waxman 1999).

At the early stages of the afterglow, as the energy density of the surrounding matter swept by the external shock wave equals the energy density of the reball plasma, a reverse shock crosses the reball plasma (Meszaros, Rees & Papathanassiou 1994; Sari & Piran 1995). At this transition phase, lasting over a duration comparable to that of the burst itself, both forward and reverse shocks accelerate particles, which subsequently emit the early afterglow. Early optical emission from several GRBs has been identified as reverse shock emission (Akerlof et al. 1999; Sari & Piran (1999); Meszaros & Rees (1999); Kobayashi (2000); Kobayashi & Sari (2000); Wei (2003); Zhang, Kobayashi & Meszaros (2003)).

In the past few years, evidence accumulated for the existence of a high energy emission component (> 1 GeV to > 1 TeV) associated with gamma-ray bursts (GRBs), which are typically observed at much lower energies, few keV to few MeV. Such a component was first observed by EGRET in the 100 MeV - 18 GeV range (Schneid et al. 1992; Hurley et al. 1994). There is evidence for even higher energy, > 1 TeV emission, observed in one burst out of 54 BATSE GRBs in the MILAGRO field of view (Atkins et al. 2000, 2003).

The mechanism responsible for high energy photon emission is still controversial. High energy electrons inverse Compton (IC) scatter low energy photons to high energies, 1 GeV - 1 TeV (Meszaros, Rees & Papathanassiou 1994) extending the spectrum to high energy. The exact shape of the spectrum depends on the values of the uncertain parameters of the model (Chiang & Dermer 1999; Wang, Dai & Lu 2001; Zhang & Meszaros 2001). An additional source of high energy emission is the possible acceleration of baryons, first suggested by Waxman (1995a), Vietri (1995) and Milgrom & Usov (1995). Accelerated protons can emit synchrotron radiation at this energy band (Vietri 1997b; Totani 1998a,b; Botcher & Dermer 1998). High energy baryons can also produce energetic pions, via photo-meson interactions with the low energy photons, creating an alternative source of high energy photons and neutrinos (Waxman & Bahcall 1997, 2000; Botcher & Dermer 1998). A high energy component may also be created by the decay of energetic pions, produced in proton-proton (neutron) collisions, if the expanding plasma collides with a dense ($n \sim 10^{-11}$ cm⁻³) cloud (Katz 1994; DePaolis, Ingresso & Orlando 2000).

In this paper, we analyze the high energy emission

¹ Physics faculty, Weizmann Institute of Science, Rehovot 76100, Israel

² asaf@wicc.weizmann.ac.il

component during the early afterglow (transition phase) on a time scale of tens to hundreds of seconds following the GRB, within the framework of the reball model. We explore the dependence of photon spectrum on uncertain model parameters, in particular on the energy density of the magnetic field, the power law index of the accelerated particles and the density of the medium surrounding the reball. The ambient medium density differs widely between different scenarios for GRB production. In the neutron star merger scenario (Goodman 1986; Paczynski 1986; Eichler et al. 1989), for example, a density typical to the ISM ($n \sim 1 \text{ cm}^{-3}$) is generally expected, while in the massive stellar collapse scenario (Woosley 1993; Levinson & Eichler 1993; Paczynski 1998) a much higher density ($n \sim 10^3 - 10^4 \text{ cm}^{-3}$) may be expected in a wind surrounding the progenitor, due to mass loss preceding the collapse (Chevalier 2001). In addition, we explore the possible contribution of high energy protons.

Calculation of the early high energy emission spectrum is complicated due to several reasons: First, IC scattering is partly in the Klein-Nishina regime. Second, high energy photons (produced by IC scattering or via pion decay) initiate high energy electro-magnetic cascades, the evolution of which is difficult to study analytically. Studies of cascade processes in the past (Bonometto & Rees (1971); Guilbert, Fabian & Rees (1983); Svensson (1987)) have shown that it may have a significant effect on the spectrum at high energies. And third, the optical depth to pair production may be large at high energy, leading to the formation of a large number of e^+e^- pairs which affect the resulting spectra. Due to these complications, numerical calculations are required to accurately determine the high energy spectra and their dependence on uncertain model parameters.

Numerical methods were extensively used in the past in the study of active galactic nucleus (AGN) plasma (Guilbert, Fabian & Rees 1983; Zdziarski & Lightman 1985; Fabian et al. 1986; Lightman & Zdziarski 1987; Coppi 1992). Using these methods, new results were obtained, such as the complex pattern of the spectral indices in the X-ray ($2 - 10 \text{ keV}$) range, that were not obtained by previous analytic calculations. In the context of the high energy emission from GRB's, numerical calculations are challenging. The large difference between the characteristic time scales for the evolution of high energy and low energy particles, and the fact that the distribution of low energy particles evolves on a time scale comparable to the dynamical time and does not reach a steady-state, implies that the numerical code must follow processes characterized by widely differing time scales. Due to these difficulties, the accuracy of existing numerical calculations of emission from GRB's (Panaitescu & Meszaros 1998) is limited above 1 GeV . Here we present numerical results using a code that allows to overcome the difficulties mentioned above. Our time dependent model includes an accurate description of synchrotron emission, direct and inverse Compton scattering, pair production and the evolution of high energy electromagnetic cascades.

Several new high energy photon detectors will become fully operational in the near future. These in-

clude the GLAST³ satellite, which will greatly improve the sensitivity at 1 GeV and will open a new window of observation up to 100 GeV . GLAST sensitivity, $10^{-13} \text{ erg cm}^{-2} \text{ sec}^{-1}$ at 1 GeV will allow detection of many hundreds of bursts per year, if GRB's emit equal amount of energy at GeV and keV bands. In addition, new generation of sub-TeV Cerenkov detectors such as MAGIC⁴, HESS⁵, VERITAS⁶ and CANGAROO III⁷ will open new era in GRB observations. The universe is transparent to 100 GeV photons up to redshift of 0.5 (e.g. Salamon & Stecker 1998). Given the local rate of GRBs (Guetta, Piran & Waxman 2003), the sensitivity of these detectors at 100 GeV , $10^{-10} \text{ erg cm}^{-2} \text{ sec}^{-1}$ for a 100 second burst, will allow a detection of few to few tens of GRB's per year at this energy band (depending on the exact instrument energy threshold) if the GRB spectrum in the keV - sub TeV range is at, $F \sim 0$. The field of view of the Cerenkov telescopes is small, which implies that fast slewing to the GRB position, on minute time scale, would be required. This may be achievable with the fast alerts that will be provided by SWIFT⁸. The sensitivity of the MILAGRO⁹ shower detector at 1 TeV would allow it to detect 1 event per year. The results presented here may therefore be useful for planning the observing strategy of the detectors and may allow to use high energy data to constrain the values of uncertain parameters of the model.

This paper is organized as follows. In §2 we derive the plasma conditions during the transition phase, which is the duration over which the reverse shock exists. We calculate the critical synchrotron frequencies and luminosities in the "wind" scenario (§2.1) and in the "uniform density ISM" scenario (§2.2). In §2.3 we discuss proton energy loss and its contribution to high energy photon emission. Our numerical model is briefly presented in §3; A detailed description of the model may be found in Peer & Waxman (2004). In §4 we present our numerical results. We summarize and conclude in §5, with special emphasis on implications for high energy photon telescopes.

2. MODEL ASSUMPTIONS, PLASMA CONDITIONS AND PROTON ENERGY LOSS AT THE TRANSITION PHASE

The interaction of reball ejecta with surrounding gas produces a reverse shock which propagates into and decelerates the reball ejecta. As the reverse shock crosses the ejecta, it erases the memory of the initial conditions, and the expansion then approaches the Blandford-McKee self-similar solutions (Blandford & McKee 1976). We derive in this section the plasma parameters, the low energy photon luminosity and spectrum, and the proton energy loss time scales expected during this transition phase, for reball expanding into a wind and into a uniform medium with density typical to the ISM.

2.1. Wind scenario

³ <http://www-glast.stanford.edu>

⁴ <http://hegralmppmunpg.de/MAGICWeb>

⁵ <http://www.mpi-hd.mpg.de/hfm/HESS/HESS.html>

⁶ <http://veritas.sao.arizona.edu/>

⁷ <http://icrh9.icrr.u-tokyo.ac.jp/>

⁸ <http://www.swift.psu.edu/>

⁹ <http://www.lanl.gov/milagro/>

The mass loss preceding a collapse creates a density profile $\rho(r) = Ar^{-2}$, where the proportionality constant is taken as $A = 5 \times 10^{11} \text{ g cm}^{-1}$, and a value of $A = 1$ is assumed for a typical Wolf-Rayet star (Willis 1991). During the self-similar expansion, the Lorentz factor of plasma behind the forward shock is $\Gamma_{BM} = (9E/16 \rho(r))^{1/2} r^{-3/2}$, where $\rho(r)$ is the energy density of the surrounding medium, $\rho(r) = (r/r_0)^{-2}$, and E is the (isotropically equivalent) recoil energy. The characteristic time at which radiation emitted by shocked plasma at radius r is observed by a distant observer is $t_r = 4 \Gamma_{BM}^2 c$ (Waxman 1997c).

The reverse shock is relativistic if the energy density of the surrounding matter swept by the forward shock equals the energy density of the propagating plasma. Since both energy densities decrease with the second power of the radius, a relativistic shock is formed if $E = (4 r^2 \rho(r) c T) = 4 \rho(r) r^2 c T$, i.e. if

$$E = 16 r^2 \rho(r) c T = 5.5 \times 10^{56} A T_{2,5}^4 \text{ erg}; \quad (1)$$

where $\rho(r) = 10^{2.5} \rho_{i,2.5}$ is the original ejecta Lorentz factor, and $T = 100 T_2$ s is the burst duration. At higher explosion energy, the reverse shock is not relativistic. Both prompt and afterglow observations suggest that $E \sim 10^{54}$ erg, implying that a relativistic reverse shock should in general be formed.

The duration T (measured in the observer frame) of the transition phase, during which the reverse shock exists, is comparable to the longer of the two time scales set by the initial conditions (Waxman 2003): The (observed) GRB duration T_{GRB} and the (observed) time T at which the self-similar Lorentz factor Γ_{BM} equals the original ejecta Lorentz factor $\rho(r)$, $\Gamma_{BM}(T) = \rho(r)$. This implies that the transition radius to self-similar expansion, $r_s = 4 \Gamma_{BM}^2 c T$, is

$$r_s = \max \left(2.2 \times 10^6 E_{53}^{1/2} T_2^{1/2} A^{1/2}; 4.4 \times 10^4 E_{53}^2 T_2^2 A^{-1} \text{ cm} \right); \quad (2)$$

where $E = 10^{53} E_{53}$ erg. During the transition, shocked plasma expands with Lorentz factor close to that given by the self-similar solution, $\Gamma_{BM}(r = r_s)$, i.e.,

$$\Gamma_{BM} = \frac{9E}{64 A T c^3} = 43 E_{53}^{1/4} T_2^{1/4} A^{1/4}; \quad (3)$$

The Lorentz factor of the reverse shock in the frame of the unshocked plasma is $\Gamma_r = 1/\Gamma_{BM}$.

We denote by ϵ_e and ϵ_B the fractions of the thermal energy density that are carried, respectively, by electrons and magnetic fields. The characteristic Lorentz factor of electrons accelerated at the forward shock is $\Gamma_{char,f} = \epsilon_e \Gamma_{BM} m_p m_e$. Electrons accelerated at the reverse shock are characterized by $\Gamma_{char,r} = \epsilon_e (\Gamma_r - 1) m_p m_e / \epsilon_e (\Gamma_{BM} - 1) m_p m_e$. The minimum Lorentz factor of a power law accelerated electrons is

$$\Gamma_{min} = \Gamma_{char} \left(\frac{8}{p-1} \right)^{1/p} \quad p \neq 2; \quad (4)$$

where p is the power law index of the accelerated electrons energy distribution, $n_e(E) / n_e^p$.

$$\begin{aligned} \text{Synchrotron emission peaks at } \Gamma_{min}^{ob} &= \\ (3=2) \sim \frac{2}{m_{in}} q B = m_e c. \text{ Using} \\ r &= \frac{4 A^3 c^3}{9 E T^3} = 7.0 \times 10^3 E_{53}^{1/2} T_2^{3/2} A^{3/2} \text{ erg cm}^{-3} \end{aligned} \quad (5)$$

for the energy density behind the forward shock at the transition radius, the synchrotron emission peak at the reverse and forward shocks is given by

$$\begin{aligned} \Gamma_{min,r}^{ob} &= 0.5 (1+z)^{-1} E_{53}^{1/2} T_2^{1/2} A^{2/5} \epsilon_e^{1/5} \epsilon_B^{2/5} \text{ eV}; \\ \Gamma_{min,f}^{ob} &= 20 (1+z)^{-1} E_{53}^{1/2} T_2^{3/2} \epsilon_e^{1/5} \epsilon_B^{2/5} \text{ eV}; \end{aligned} \quad (6)$$

where $p = 2$, $\log(m_{ax} = m_{in})' = 10$ assumed, $\epsilon_e = 0.1 \epsilon_e$, and $\epsilon_B = 0.01 \epsilon_B$. These energies are above Γ_{jc} , the characteristic synchrotron energy of electrons for which the synchrotron cooling time, $9 m_e^3 c^5 = 4 q^4 B^2$, is comparable to the ejecta (rest frame) expansion time, $r = c$,

$$\Gamma_{jc}^{ob} = 2.1 \times 10^2 (1+z)^{-1} E_{53}^{1/2} T_2^{1/2} A^{2/5} \epsilon_e^{1/5} \epsilon_B^{2/5} \text{ eV}; \quad (7)$$

$\Gamma_{min,r}^{ob}$ is comparable to the synchrotron self-absorption energy, below which the optical depth becomes larger than 1,

$$\Gamma_{ssa}^{ob} = 0.4 (1+z)^{-1} T_2^{-1} A^{2/3} \epsilon_e^{1/3} \epsilon_B^{1/3} \text{ eV} \quad (8)$$

(for $p = 2$). Equating the particle acceleration time, $t_{acc} = E/(qB)$ and the synchrotron cooling time, gives the maximum Lorentz factor of the accelerated electrons (in the plasma rest frame), $\Gamma_{max} = 1.8 \times 10^7 E_{53}^{1/8} T_2^{3/8} A^{1/4} \epsilon_e^{1/4} \epsilon_B^{1/4}$. Synchrotron emission from these electrons peaks at

$$\Gamma_{max}^{ob} = 1.0 \times 10^{10} (1+z)^{-1} E_{53}^{1/4} T_2^{1/4} A^{1/4} \epsilon_e^{1/4} \epsilon_B^{1/4} \text{ eV}; \quad (9)$$

The reverse shock specific luminosity $L_* = dL/d\Gamma^{ob}$ at $\Gamma_{min,r}^{ob}$ is

$$L_m = 2.8 \times 10^{60} E_{53}^{3/2} T_2^{1/2} A^{1/5} \epsilon_e^{1/5} \epsilon_B^{1/5} \text{ s}^{-1}; \quad (10)$$

For a power law energy distribution with $p = 2$ of the accelerated electrons, the specific luminosity is $L_* / \Gamma^{1/2}$ above $\Gamma_{min,r}$.

2.2. Uniform density ISM

During self-similar expansion into uniform density medium, the Lorentz factor of plasma is given by $\Gamma_{BM} = 17E/16 n_p c^2 r^{-3/2}$ (Blandford & McKee 1976). The transition to self-similar expansion occurs at a radius

$$r_s = \max \left(6.3 \times 10^6 E_{53}^{1/3} n_0^{1/3} \epsilon_e^{2/3}; 1.3 \times 10^7 E_{53}^{1/4} n_0^{1/4} T_2^{1/4} \text{ cm} \right); \quad (11)$$

where a typical value $n = 1 n_0 \text{ cm}^{-3}$ of the ambient number density assumed. Calculations of the characteristic Lorentz factors, synchrotron frequencies and characteristic luminosities closely follow the steps of the wind scenario calculations, and partly appear in

Waxman & Bahcall (2000). The peak energy of synchrotron emission from electrons accelerated at the reverse shock,

$$\epsilon_{\text{peak}}^{\text{ob}} = 2 \cdot 10^2 (1+z)^{-1} n_0^{1=2} \epsilon_{i;2;5}^2 \epsilon_{e;1}^{1=2} \epsilon_{B;2} \text{ eV}; \quad (12)$$

is comparable to the synchrotron self-absorption energy,

$$\epsilon_{\text{ssa}}^{\text{ob}} = 5 \cdot 10^2 (1+z)^{-1} E_{53}^{1=3} n_0^{1=3} T_2^{2=3} \epsilon_{e;1}^{1=3} \epsilon_{B;2}^{1=3} \text{ eV}; \quad (13)$$

and is below

$$\epsilon_{\text{rc}}^{\text{ob}} = 10 (1+z)^{-1} E_{53}^{1=2} n_0^{1=2} T_2^{1=2} \epsilon_{B;2}^{3=2} \text{ eV}; \quad (14)$$

Synchrotron emission from electrons accelerated at the forward shock peaks at higher energy,

$$\epsilon_{\text{mf}}^{\text{ob}} = 25 (1+z)^{-1} E_{53}^{1=2} T_2^{3=2} \epsilon_{e;1}^{2=2} \epsilon_{B;2}^{1=2} \text{ eV}; \quad (15)$$

The reverse shock specific luminosity, $L_{\text{r}} = dL/d\epsilon^{\text{ob}}$ at ϵ_{rc} is

$$L_{\text{r}} = 1.5 \cdot 10^{59} E_{53}^{3=2} T_2^{1=2} n_{e;1}^{3=2} \epsilon_{B;2} \text{ s}^{-1}; \quad (16)$$

For a power law energy distribution with $p = 2$ of the accelerated electrons, $L_{\text{r}} / \epsilon^{-1}$ at higher energies, $\epsilon > \epsilon_{\text{rc}}$.

2.3. Proton energy loss and its contribution to high energy photon emission

Protons accelerated to high energy in the reverse shock contribute to the emission of high energy photons by synchrotron emission and photo-production of pions, which decay to produce high energy photons and electrons (and neutrinos). The maximum energy to which protons are accelerated is determined by equating the proton acceleration time (in the plasma frame), $t_{\text{acc}} \sim p m_p c^2 = \alpha B$, to the minimum of the dynamical time, the synchrotron energy loss time, and the pion production energy loss time. For expansion into a wind, the acceleration time is equal to the dynamical time, $T_{\text{dyn}} = 4 T$, for protons with (plasma frame) Lorentz factor

$$p_{\text{dyn}} \sim 2 \cdot 10^0 A^{1=2} \epsilon_{B;1}^{1=2}; \quad (17)$$

and to the synchrotron loss time, $t_{\text{syn}} = 9m_p^3 c^5 = 4\alpha^4 B^2 p$, for protons with (plasma frame) Lorentz factor

$$p_{\text{syn}} \sim 2 \cdot 10^0 E_{53}^{1=8} T_2^{3=8} A^{3=8} \epsilon_{B;1}^{1=4}; \quad (18)$$

The time for energy loss via pion production may be approximated as (Waxman & Bahcall 1997)

$$t^{-1} = \frac{1}{2} \frac{Z_1}{p} c \frac{d\sigma}{d\epsilon} \frac{dN}{d\epsilon} \frac{d\epsilon}{d\epsilon} \frac{dx}{dx} \frac{2n(x)}{n(x)}; \quad (19)$$

σ is the cross section for pion production for a photon with energy ϵ in the proton rest frame, $\langle \epsilon \rangle$ is the average fraction of energy lost to the pion, and $\epsilon_0 = 0.15 \text{ GeV}$ is the threshold energy. The specific photon density, $n(x)$, is related to the observed luminosity by $n(x) = L_{\text{r}}(x) / 4\pi r^2 c x$. Photo-meson production is dominated by interaction with photons in the energy range $\epsilon^{\text{ob}} > \epsilon_0 = 2 p_{\text{dyn}} \epsilon_{\text{mf}}^{\text{ob}}$, where $L_{\text{r}} / \epsilon^{-1}$, thus

$$t^{-1} = \frac{2}{3} \frac{L_{\text{m}}}{r^2} \frac{p}{2} \frac{\epsilon_{\text{peak}}^{\text{ob}}}{\epsilon_{\text{peak}}} \frac{\epsilon_{\text{peak}}^{\text{peak}}}{\epsilon_{\text{peak}}}; \quad (20)$$

A contribution from the π -resonance comparable to that of photons of higher energy was assumed in evaluating the first integral. Using $\epsilon_{\text{peak}}^{\text{peak}} \sim 5 \cdot 10^{28} \text{ cm}^2$ and $\epsilon_{\text{peak}}^{\text{peak}} \sim 0.2$ at the resonance $\epsilon = \epsilon_{\text{peak}} = 0.3 \text{ GeV}$, and $\epsilon_{\text{peak}}^{\text{peak}} \sim 0.2 \text{ GeV}$ for the peak width, the acceleration time equals the pion production loss time for protons with (plasma frame) Lorentz factor

$$p_{\text{r}} \sim 4.6 \cdot 10^8 E_{53}^{1=8} T_2^{3=8} A^{3=8} \epsilon_{e;1}^{1=2} \epsilon_{B;1}^{1=4}; \quad (21)$$

Comparing eqs. (17), (18) and (21) we find that proton acceleration is limited by energy losses, and that pion production losses dominate over synchrotron losses for

$$\epsilon_e \text{ \& } \epsilon_B = 10; \quad (22)$$

Note, that this is valid independent of the proton energy, since $t / t_{\text{syn}} \sim p^{-1}$. X-ray afterglow observations suggest that ϵ_e is close to equipartition, $\epsilon_e \sim 1=3$ (Friedman & Waxman 2001; Berger, Kulkarni & Frail 2003). Thus, we expect proton energy losses to be dominated by pion production. Comparing eqs. (17) and (21) we find that for $\epsilon_e \sim 0.1$ the highest energy protons lose all their energy to pion production. Assuming a power law distribution of proton energies, $dn_p/dp \sim p^{-2}$, roughly 0.1 of the energy carried by protons will be converted in this case to pions, and roughly half of this energy would be converted to high energy photons through the decay to photons and electrons (positrons). Since shock accelerated electrons lose all their energy to radiation, this implies that the contribution of protons to the luminosity is similar to that of the electrons. This is valid also for values of ϵ_e well below equipartition, $\epsilon_e \sim 0.1$, since the contribution to the luminosity of both electrons and protons is $\sim \epsilon_e^{-1}$ in this case.

In the case that eq. (22) is not satisfied, and the proton energy loss is dominated by synchrotron losses, comparing eqs. (17) and (18) implies that the highest energy protons lose all their energy to synchrotron losses if the magnetic field is close to equipartition. For lower values of ϵ_B , the highest energy protons lose a fraction $\epsilon_B^{3=2}$ of their energy by synchrotron emission. In this case, proton synchrotron emission would dominate the electron luminosity if $\epsilon_B^{3=2} > 10 \epsilon_e$.

For explosion into a uniform density ISM, similar arguments imply that pion production losses dominate over synchrotron losses when eq. (22) is satisfied. Following the analysis of Waxman & Bahcall (2000), protons which are expected to be accelerated up to p_{dyn}

$5 \cdot 10^8 E_{53}^{1=4} n_0^{1=4} T_2^{1=4} \epsilon_{B;1}^{1=2}$, lose a fraction $f(p)$ $2 \cdot 10^{11} p E_{53}^{3=8} n_0^{5=8} T_2^{1=8} \epsilon_{e;1}$ of their energy to pion production. Therefore, for a power law index $p = 2$ of the accelerated protons, pions receive a fraction $\sim 10^{-3} E_{53}^{5=8} n_0^{7=8} T_2^{1=8} \epsilon_{e;1}^{1=2} \epsilon_{B;1}$ of the total proton energy. Since in this scenario as well electrons lose almost all their energy to radiation, the total proton contribution to the photon flux is $\sim 5 \cdot 10^3$ of the electron contribution, independent on the value of ϵ_e . If eq. (22) is not satisfied, proton synchrotron losses dominate over pion production. A similar calculation to the former case shows that proton synchrotron emission dominates the electron luminosity in this scenario only if $\epsilon_B^{3=2} > 10^4 \epsilon_e$.

The discussion presented above demonstrates that the energy loss of protons is expected to be dominated by

pion production, and that this energy loss may produce a luminosity similar to that of the electrons in the scenario of explosion into a wind. Finally, it should be pointed out that if protons are accelerated to a power-law energy distribution with an index p significantly larger than 2, their contribution to the luminosity will be significantly reduced, since the fraction of energy carried by the highest energy protons will be small.

3. THE NUMERICAL MODEL

The acceleration of particles in the two shock waves that exist during the transition phase is accompanied by numerous radiative processes. In the numerical calculations, we use the time dependent numerical model described in Pe'er & Waxman (2004). Our time dependent model follows the evolution of the particle distribution and the emergent spectra, by solving the kinetic equations for the electron and photon distributions, taking into account synchrotron emission, inverse Compton scattering, pair production and pion photo-production interactions. These calculations are done for a wide range of particle energies, including the evolution of rapid electro-magnetic cascades at high energies.

In the calculations, we focus on particles that pass through the forward or the reverse shock waves and therefore are in the downstream region of the flow, relative to the relevant shock wave. While the upstream relativistic flow is highly anisotropic, the shocked gas thermalize, hence isotropise (in the plasma comoving frame) immediately after passing the shock, on a characteristic length scale of several skin-depth (e.g., Kirk et al. 1998, 2000; Frederiksen et al. 2004). The emitted radiation is therefore isotropic in the comoving frame. Most of the shocked gas and most of the blast-wave energy are concentrated in a shell of comoving thickness $r = cT_{\text{dyn}}$ with $\beta \approx 1$ (e.g., in the Blandford & McKee (1976) self-similar solutions which give the spatial dependence of the hydrodynamical variables, 90% of the energy is concentrated in a shell of comoving thickness corresponding to $\beta = 1-7$). Since the details of the spatial dependence of the electron and magnetic field energy fractions are not known, we adopt in our model the commonly used approximation (e.g., Lightman & Zdziarski 1987; Coppi 1992; Pilla & Loeb 1998) that radiation is produced within a homogeneous shell of comoving width $r = cT_{\text{dyn}}$ with $\beta = 1$. Since the shocks velocity is time independent during T_{dyn} , the shock-heated comoving plasma volume is assumed to increase linearly with time, i.e., constant particle number density is assumed (see Pe'er & Waxman 2004, for further details).

In the comoving frame, homogeneous and isotropic distributions of both particles and photons are therefore assumed. Parallel calculations of processes in the two shock waves are carried out, where photons produced at each shock participate in IC scattering, photo-production interactions and pair production interactions occurring at both shocks.

The particle distributions are discretized, the proton spectrum spans 11 decades of energy ($p < 10^{11}$), and the electron spectrum 14 decades ($e < 10^{14}$). A fixed time step is chosen, typically 10^{-4} times the dynamical time. Numerical integration is carried out with this fixed time step. Particles and photons for which the energy loss time or annihilation time are shorter than the fixed

time step, are assumed to lose all their energy in a single time step, producing secondaries which are treated as a source of lower energy particles. Photo-pion production is calculated at each time step by direct integration of the second integral in Eq. 19, while approximating the first integral by the contribution from the π^0 -resonance (see the discussion following Eq. 20). Half of the energy lost by protons goes into π^0 that decays into 2 photons, each carrying 10% of the initial proton energy.

The following approximations are made: (i) Plasma parameters are assumed to be time independent during the transition phase; (ii) The fraction of thermal energy that is carried by electrons (magnetic field), ϵ_B (ϵ_B), is the same at the forward and reverse shock waves; (iii) The power law index of the energy distribution of accelerated electrons and protons is the same at both shocks.

In the present calculations, we do not consider proton synchrotron emission, which is dominated by pion production for the considered parameter range. Synchrotron self absorption is also not considered here, being irrelevant for processes occurring at high energies. Photons below the self absorption frequency, $\nu_{\text{ssa}}^{\text{obs}} \approx 1 \text{ eV}$ (in both scenarios; see eqs. 8, 13) can produce pairs only with photons energetic than $2(m_e c^2)^2 = \nu_{\text{ssa}}^{\text{obs}} \approx 10^{16} \text{ eV}$, which are absent (see the numerical results below). Moreover, these photons are below the threshold energy for pion production, $\nu_{\text{TH}}^{\text{obs}} \approx 0.2 \text{ GeV} = \gamma_p = 10 \text{ eV}$, where $\gamma_p = 5 \times 10^9$ (see eq. 21), and $\gamma = 10^{2.5}$ were taken.

4. NUMERICAL RESULTS

4.1. High vs. low density

Figure 1 shows spectra obtained from a GRB transition phase in the two scenarios discussed: Explosion in a uniform low density medium typical to the ISM, $n = 1 \text{ cm}^{-3}$, and explosion in a $A = 1$ wind, where the density of ambient medium at the transition radius is much higher, $n = 10^3 \text{ cm}^{-3}$.

The most evident feature of the two spectra is their anisotropy, $F \propto \gamma^2$ with $\gamma > 0$, extending over seven energy decades between $\nu_{\text{min}}^{\text{obs}} \approx 1.4 \text{ keV}$ and $\nu_{\text{max}}^{\text{obs}} \approx 60 \text{ GeV}$ for expansion into ISM, and over ten energy decades from $\nu_{\text{min}}^{\text{obs}} \approx 1 \text{ eV}$ to $\nu_{\text{max}}^{\text{obs}} \approx 10 \text{ GeV}$ for explosion into a wind. This is a result of dominant synchrotron emission term at these energies.

The main difference between the two scenarios appears at high energies, $100 \text{ GeV} - 1 \text{ TeV}$, due to the different optical depth to pair production, τ_{pair} , as shown in Figure 2. The large optical depth to pair production in the wind case softens the high energy IC spectrum, resulting in spectral index $\alpha = 1$. Consequently, while in the ISM case the 1 TeV flux is comparable to the flux at 1 GeV , in the high density wind case the 1 TeV flux is 2.5 orders of magnitude lower. A second difference between the two scenarios appears at the optical-UV band. In the low density scenario, at low energies, $\nu_{\text{min}}^{\text{obs}} \approx 1 \text{ eV}$, emission from both shock waves produces a moderate increase in the spectral slope, $\alpha \approx 0.3$ above $\nu_{\text{IC}}^{\text{obs}} \approx 20 \text{ eV}$. As demonstrated in Figure 3, this slope results from a flat spectrum produced at the reverse shock, $\alpha = 0$ above $\nu_{\text{min}}^{\text{obs}} \approx 10^2 \text{ eV}$, and forward shock emission characterized by $\alpha = 0.5$ below $\nu_{\text{min}}^{\text{obs}} \approx 1 \text{ eV}$. In a high density medium, a nearly flat spectrum is obtained above $\nu_{\text{min}}^{\text{obs}} \approx 1 \text{ eV}$.

In an explosion into constant density ISM scenario, the total energy carried by the IC scattered photons is $\sim 10\%$ of the total energy in synchrotron emitted photons, well below the simple estimate $(\epsilon_e/\epsilon_B)^{1/2}$, which is based on the assumption that all the synchrotron emitted photons serve as seed photons for Compton scattering. This discrepancy is due to Klein-Nishina suppression of the cross-section at high energies. Consequently, IC scattering becomes dominant only above ~ 50 GeV, where a tail spectrum is created for a power law index $p = 2$ of the accelerated electrons energy distribution. In the wind case, IC scattering is more prominent due to the higher photon density.

Lightcurve of the spectrum of an explosion into constant density ISM scenario is presented in Figure 4. The constant injection rate of energetic electrons results in a linear increase of the synchrotron emission component in time. Since the energy of photons emitted by electrons for which the synchrotron cooling time equals the time t , $\gamma_c(t)/t^2$, the energy density in the low energy photons increases with time. Only photons with $\epsilon_{\text{obs}} \sim 1$ keV are in the Thompson limit for Compton scattering, therefore the inverse Compton component increases in time, at early times. At later times, $t \sim T_{\text{dyn}}$, where $T_{\text{dyn}} = 4 R_{\text{BM}}/c$ is the dynamical time of the problem, the low energy photon density becomes high enough that pair production phenomenon limits the high energy emission component.

The contribution of protons to the photon flux is negligible in the ISM case, however this contribution is 85% of the electrons' contribution to the flux in the wind scenario (see x2.3). Most of this contribution results from the decay of energetic pions, initiating high energy electro-magnetic cascades. The high energy cascade results in a flat ($\alpha = 0$) spectrum at the observed energy range, which, for power law index of the accelerated particles $p = 2$ is similar to the spectrum from inverse Compton scattering. An additional small contribution from the decay of low energy pions results in a spectral slope $\alpha = 1$, contributing to the small deviation from flat spectrum shown below 1 GeV in this scenario. Above the energy at which the optical depth for pair production $\tau_{\gamma\gamma} > 1$, ~ 1 GeV, the spectrum is determined by the spectrum of low energy photons, thus the proton contribution is hard to discriminate at these energies as well.

4.2. Fraction of energy carried by electrons and magnetic field

In an explosion into a low density ISM, $\epsilon_{\text{mag}}/\epsilon_{\text{e}} < \epsilon_{\text{max}}/\epsilon_{\text{c}}$. Thus, for $p' > 2$ electrons lose nearly 100% of their energy to radiation, resulting in a nearly linear dependence of the flux on ϵ_e . The dependence of the spectrum on the fraction of thermal energy carried by the magnetic field, ϵ_B , is illustrated in Figure 5. The domination of synchrotron emission implies that the values of γ_c and γ_m determine the spectral behavior at low energies, while a tail spectrum is expected for $p = 2$ at higher energies, up to $\epsilon_{\text{max}} \sim 50$ GeV. The ratio of 1 GeV to 1 keV flux is informative about the value of ϵ_B , with large ratio (~ 30) implying small ϵ_B ($\sim 10^{-4}$). At higher energies, $\epsilon > 100$ GeV, a flux comparable to the 1 GeV flux is produced by IC scattering for $\epsilon_B < 0.1$.

For explosion into a wind, $\epsilon_{\text{c}} < \epsilon_{\text{mag}}/\epsilon_{\text{e}} < \epsilon_{\text{max}}/\epsilon_{\text{c}}$. Here too,

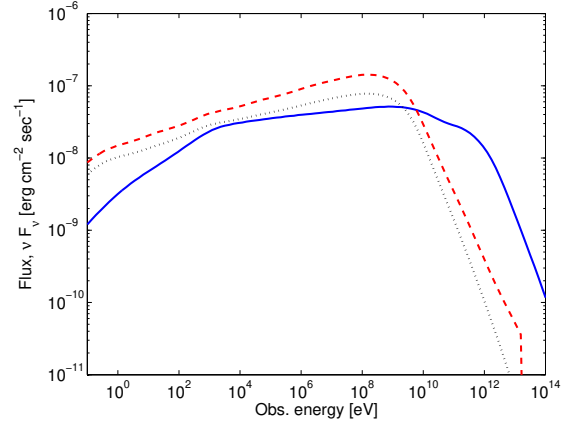


Fig. 1. Predicted photon spectrum during the transition phase. Results are shown for $E = 3 \cdot 10^{53}$ erg, $\epsilon_i = 10^{2.5}$, $T = 10$ s, $\epsilon_e = 10^{-1}$, $\epsilon_B = 10^{-2}$, $p = 2.0$. Solid: explosion into uniform low density medium (ISM), $n = 1 \text{ cm}^{-3}$. Dashed: Explosion into a wind with $A = 1 \text{ g cm}^{-1}$. Dotted: Explosion into a wind with $A = 1 \text{ g cm}^{-1}$, proton contribution to the flux omitted. Luminosity distance $d_L = 2 \cdot 10^{28}$ cm and $z = 1$ were assumed. Inter-galactic absorption of high energy photons through pair production interactions with the IR background, which becomes appreciable above ~ 0.1 TeV, is not taken into account.

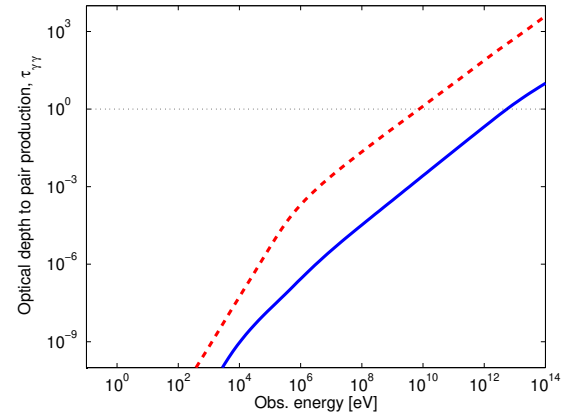


Fig. 2. Energy dependent optical depth to pair production, for the two scenarios considered in Figure 1. Solid: explosion into ISM, dashed: explosion into a wind. All physical parameters are the same as in Figure 1.

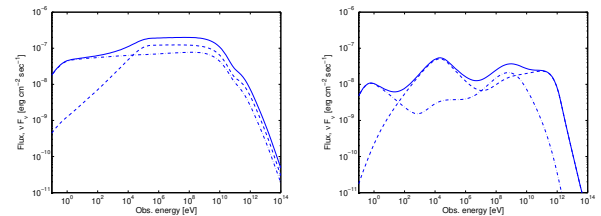


Fig. 3. Two emission components of the observed spectra, explosion into ISM. Dash: forward shock emission, dash-dotted: reverse shock emission, solid: combined spectra. Left: equipartition, $\epsilon_e = 10^{-0.5}$, $\epsilon_B = 10^{-0.5}$, $p = 2.0$. The two emission components are comparable. Right: $\epsilon_e = 10^{-1}$, $\epsilon_B = 10^{-2}$, $p = 3.0$. The wavy shape results from different peaks of the two synchrotron components, and the two IC components. All other physical parameters are the same as in Figure 1.

for $p' > 2$ electrons lose nearly 100% of their energy to radiation, resulting in a nearly linear dependence of flux on ϵ_e . The dependence of the spectrum on ϵ_B is illustrated

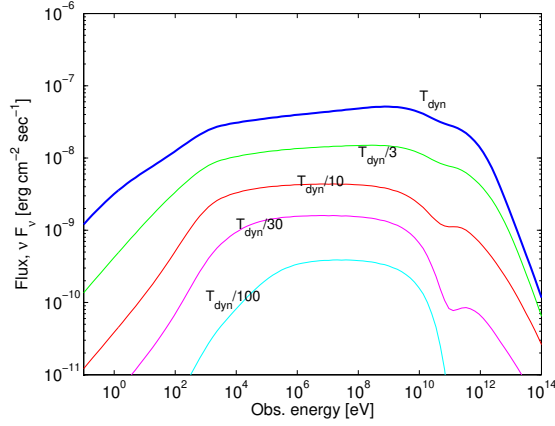


Fig. 4. Lightcurve of the spectra for the scenario of explosion into uniform low density medium (same parameters as in figure 1). The lines show the spectrum after fractions of 1/100, 1/30, 1/10, 1/3 and 1 dynamical time.

in Figure 6. Here, IC emission is much more prominent. IC energy loss of the electrons affects the spectrum at all energy bands by modifying the electrons energy distribution. The spectrum becomes harder with lower values of B , reaching 0.2 below 10 GeV for $B = 10^4$. In this scenario, the minimum Lorentz factor of electrons accelerated at the front shock, $\gamma_{min,f} = 2 \cdot 10^3$ (see Eq. 4) is comparable to $\gamma_{IC,s} = 10^4$, which is defined as the Lorentz factor of electrons that emit synchrotron radiation above their Klein-Nishina limit. We show in Appendix A that in this case, if the main energy loss mechanism is inverse Compton scattering, a spectral index in the range $0.2 \leq \alpha \leq 0.3$ should be expected. A 1 GeV to 1 keV flux ratio larger than 10 indicates therefore $B = 10^4$, and smaller ratio indicates higher value of B , similar to the case of explosion into low density ISM. Above 10 GeV, the flux is suppressed by pair production.

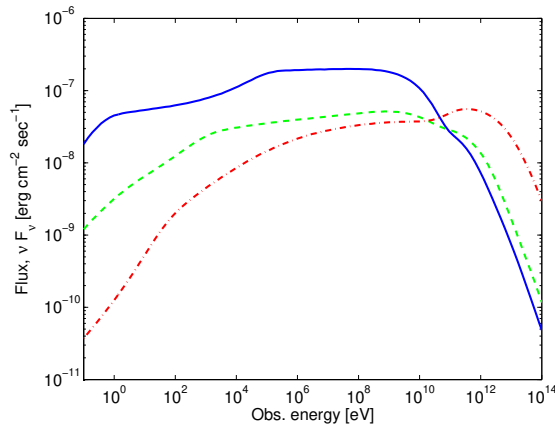


Fig. 5. Dependence of the spectra on the fraction of thermal energy carried by the electrons and by the magnetic field, ϵ_e and B , explosion into a low density ISM, $n = 1 \text{ cm}^{-3}$. Solid: $\epsilon_e = 10^{-0.5}$, $B = 10^{-0.5}$, dashed: $\epsilon_e = 10^{-1}$, $B = 10^{-2}$, dash-dotted: $\epsilon_e = 10^{-1}$, $B = 10^{-4}$. All other physical parameters are the same as in figure 1.

4.3. Power law index of the accelerated particles

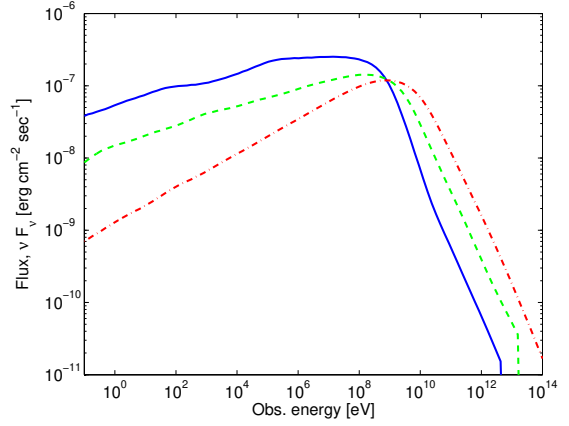


Fig. 6. Dependence of the spectra on the fraction of thermal energy carried by the electrons and by the magnetic field, ϵ_e and B , explosion into a wind characterized by $A = 1 \text{ g cm}^{-1}$. Solid: $\epsilon_e = 10^{-0.5}$, $B = 10^{-0.5}$, dashed: $\epsilon_e = 10^{-1}$, $B = 10^{-2}$, dash-dotted: $\epsilon_e = 10^{-1}$, $B = 10^{-4}$. All other physical parameters are the same as in figure 1.

The dependence of the spectrum on p varies with the external density, as demonstrated in Figures 7 and 8. The dominant synchrotron component in explosion into a low density ISM results, for large p , in a complex wavy shape shown in Figure 7. The four peaks result from synchrotron and IC components at the two shock waves, as demonstrated in Figure 3 (right). The dependence on p is, however, not prominent. For explosion into a wind, the prominent IC component leads to a spectrum which is nearly independent on p .

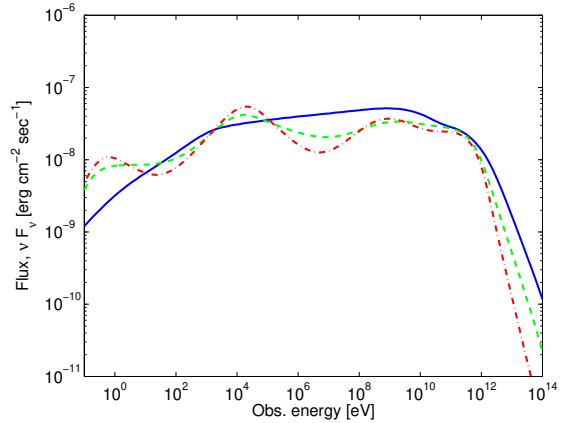


Fig. 7. Dependence of the spectra on the power law index p of the accelerated electrons, explosion into low density ISM, $n = 1 \text{ cm}^{-3}$. Solid: $p = 2.5$, dashed: $p = 2.5$, dash-dotted: $p = 3.0$. All other physical parameters are the same as in figure 1. The wavy shape of the spectrum results from synchrotron and IC components of the two shock waves, as seen in figure 3.

5. DISCUSSION

We have presented numerical results of calculations of the early afterglow GRB spectra (figures 1, 5-8) within the reball model framework. Our time dependent numerical code describes synchrotron emission, inverse-Compton scattering, e⁺e⁻ pair production, photo-pion production and the resulting high energy cascades. We have shown that the dependence of the spectra on the

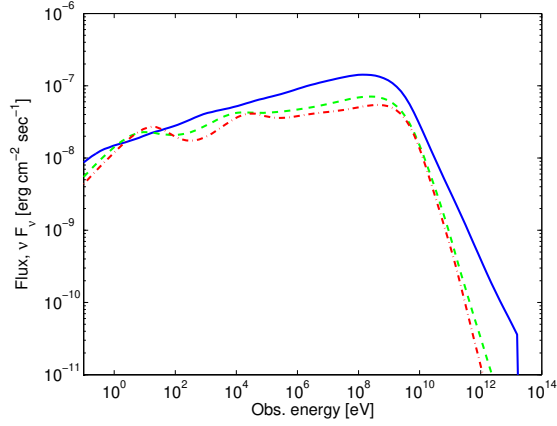


Fig. 8. Dependence of the spectra on the power law index p of the accelerated electrons, explosion into a wind with $A = 1 \text{ g cm}^{-1}$. Solid: $p = 2.0$, dashed: $p = 2.5$, dash-dotted: $p = 3.0$. All other physical parameters are the same as in figure 1.

ambient density and the magnetic field equipartition fraction is pronounced mainly at high photon energies, $1 \text{ GeV} - 1 \text{ TeV}$ (see Figures 5, 6): Comparable flux at 1 GeV and 1 TeV implies low density and $B \propto 10^4$, while a large ratio of 10^3 results from dense medium and B near equipartition. A second indication for $B \propto 10^4$ is a large (~ 30) ratio of the flux at 1 GeV to the flux at 1 keV . In all cases, the spectra depend only weakly on the power-law index p of the accelerated electrons. The flux expected in the $1 - 50 \text{ GeV}$ energy band, $F \sim 10^8 - 10^7 \text{ erg cm}^{-2} \text{ sec}^{-1}$ for $z = 1$ bursts, is well within the detection capability of GLAST.

The recent detection by MILAGRITO of 1 TeV photon flux associated with GRB 970417a (Atkins et al. 2003) can be explained as due to the onset of reball deceleration by a medium with density typical to the ISM, provided that the magnetic field is well below equipartition, $B \ll 10^4$. The flux at 1 TeV is expected in this case to be an order of magnitude higher than the 100 keV (BATSE) flux, as inferred from the MILAGRITO detection. We note, that an alternative explanation was suggested for the 1 TeV flux, synchrotron emission from shock accelerated protons (Totani 1998a,b). This explanation requires a very low fraction of the energy to be

carried by electrons, $\epsilon_e \sim 10^{-3}$, and an isotropic equivalent explosion energy $E \sim 10^{56} \text{ erg}$. We find this explanation less attractive, since X-ray afterglow observations imply ϵ_e values near equipartition and isotropic equivalent energies in the range of $10^{51.5} \text{ erg}$ to $10^{53.5} \text{ erg}$ (Freedman & Waxman 2001; Berger, Kulkarni & Frail 2003).

The energy loss of high energy protons is dominated by photo-production of pions, rather than by synchrotron emission, for $\epsilon_e > B = 10$. The contribution of pion decay to the high energy photon luminosity may be comparable to that of inverse-Compton emission of shock accelerated electrons in the case of reball expansion into a high density wind, and power law index $p' \sim 2$ of the accelerated particles. However, it is difficult to distinguish in this case between the electron and proton contributions since the spectral shape is determined primarily by the energy dependence of the pair production optical depth. In the two scenarios considered, explosion into constant density ISM and into a pre-ejected wind, if $\epsilon_e \sim 10^{-5} - 10^{-4}$, proton synchrotron emission becomes the dominant emission mechanism.

Although the MILAGRITO detection is singular, the new generation of high energy sub-TeV detectors, such as MILAGRO, VERITAS, HEGRA, HESS, and MAGIC that will become fully operational in the next few years, will be sensitive enough to observe the high energy early afterglow emission at 100 GeV from ~ 10 bursts per year. The detection rate of higher energy, 1 TeV component is much lower, due to the large pair production optical depth for TeV photons originating at $z > 0.3$ (e.g., Salamón & Stecker 1998). However, the predicted 1 TeV flux implies that 1 burst per year, that arrives from low redshift $z \sim 0.3$, could be detected in the 1 TeV band as well. Such detections will allow to constrain two of the uncertain parameters of the reball model: the ambient gas density, and the magnetic field equipartition fraction.

This work was supported in part by a Minerva grant and an ISF grant. AP wishes to thank Amir Sagiv for valuable discussions.

APPENDIX

SPECTRAL DISTRIBUTION RESULTING FROM SYNCHROTRON RADIATION AND IC SCATTERING

If inverse Compton scattering is the dominant energy loss mechanism of electrons that were accelerated with a power law energy distribution $dn_e = dN/dE$, the resulting power law index of energetic electrons above $\gamma_{\text{min}}(\gamma_c)$ deviates from $p+1$.

The resulting power law can be calculated analytically if the minimum Lorentz factor of the accelerated electrons γ_{min} , is comparable to γ_{ICS} , which is defined to be the Lorentz factor of electrons that emit synchrotron radiation at the Klein-Nishina limit, $\sim (3qB/2\gamma_{\text{ICS}}^2) = (2m_e c^2) = 3 = 4(m_e c^2) = \gamma_{\text{ICS}}$. At steady state, a broken power law is expected with index $(p_1 + 1)$ above γ_{ICS} and $(p_2 + 1)$ at lower energies. Synchrotron emission has a broken power law spectrum:

$$\begin{aligned} \frac{dn}{dE} &= \frac{dn}{dE} \bigg|_{p_1=2} \quad \text{for } E > E_{\text{ICS}}; \\ \frac{dn}{dE} &= \frac{dn}{dE} \bigg|_{p_2=2} \quad \text{for } E < E_{\text{ICS}}; \end{aligned} \quad (\text{A1})$$

where $E_{\text{ICS}} \sim (3qB/2\gamma_{\text{ICS}}^2) = (2m_e c^2)$. Energetic electrons therefore lose energy at a rate $dE/dt = \gamma^2 U / (1 + p_2/2)$. As these electrons are injected with power law index p , their steady distribution is $dn_e(E > E_{\text{ICS}}) = dN/dE \propto E^{-(p+p_2/2)}$, or

$$p_1 = p + \frac{p_2}{2} - 1: \quad (\text{A2})$$

At lower energies, electrons lose energy by scattering photons above ϵ_{IC} , thus $dn_e(\epsilon < \epsilon_{IC}) = d\epsilon / \epsilon^{(1+p_1=2)}$, or

$$p_2 = \frac{p_1}{2} : \quad (A3)$$

Combined together, one obtains

$$\begin{aligned} p_1 &= \frac{4}{3}(p_2 - 1); \\ p_2 &= \frac{2}{3}(p_2 - 1): \end{aligned} \quad (A4)$$

As an example, assuming power law index $p = 2$ of the accelerated electrons, the photons spectral index is $1/3$ at low energies, or $F \propto \epsilon^{-2/3}$.

Note that the above analysis is valid provided both $p_1, p_2 < 2$, which is translated via eq. (A4) into the demand $p < 2.5$.

REFERENCES

- Akerlof, C.W., et al. 1999, *Nature*, 398, 400
 Atkins, R., et al. 2000, *ApJ*, 533, L119
 Atkins, R., et al. 2003, *ApJ*, 583, 824
 Berger, E., Kulkarni, S.R., & Frail, D.A. 2003, *ApJ*, 590, 379
 Blandford, R.D., & McKee, C.F. 1976, *Phys. Fluids* 19, 1130
 Bonometto, S., & Rees, M.J. 1971, *MNRAS*, 152, 21
 Botcher, M., & Demmer, C.D. 1998, *ApJ*, 499, L131
 Chiang, J., & Demmer, C.D. 1999, *ApJ*, 512, 699
 Chevalier, R.A., 2001, in *GRB in the afterglow era*, Proceedings of the International workshop held in Rome, CNR (astro-ph/0102212)
 Coppi, B.S. 1992, *MNRAS*, 258, 657
 De Paolis, F., Ingresso, G., & Orlando, D. 2000, *A & A*, 359, 514
 Eichler, D., Livio, M., Piran, T., & Schramm, D.N. 1989, *Nature*, 340, 126
 Fabian, A.C., Blandford, R.D., Guilbert, P.W., Phinney, E.S., & Cuellar, L. 1986, *MNRAS*, 221, 931
 Frederiksen, J.T., Hededal, C.B., Haugbølle, T., & Nordlund, A. 2004, *ApJ*, 608, L13
 Freedman, D.L., & Waxman, E. 2001, *ApJ*, 547, 922
 Goodman, J. 1986, *ApJ*, 308, L47
 Gruzinov, A., & Waxman, E. 1999, *ApJ*, 511, 852
 Guetta, D., Piran, T., & Waxman, E. 2003, *ApJ*, 619, 412
 Guilbert, P.W., Fabian, A.C., & Rees, M.J. 1983 *MNRAS*, 205, 593
 Halzen, F. 1999, in *Proc. 17th Int. Workshop on weak interactions and Neutrinos*, Cape Town, South Africa (astro-ph/9904216)
 Hurley, K. et al. 1994, *Nature*, 372, 652
 Katz, J.I. 1994, *ApJ*, 432, L27
 Kirk, J.G., Rieger, F.M., & Mastichiadis, A. 1998, *A & A*, 333, 452
 Kirk, J.G., Guthmann, A.W., Gallant, Y.A., & Achterberg, A. 2000, *ApJ*, 542, 235
 Kobayashi, S. 2000, *ApJ*, 545, 807
 Kobayashi, S., & Sari, R. 2000, *ApJ*, 542, 819
 Levinson, A., & Eichler, D. 1993, *ApJ*, 418, 386
 Lightman, A.P., & Zdziarski, A.A. 1987, *ApJ*, 319, 643
 Meszaros, P. 2002, *ARA & A*, 40, 137
 Meszaros, P., & Rees, M.J. 1997, *ApJ*, 476, 232
 Meszaros, P., & Rees, M.J. 1999, *MNRAS*, 306, L39
 Meszaros, P., Rees, M.J., & Papathanassiou, H. 1994, *ApJ*, 432, 181
 Milgrom, M., & Usov, V. 1995, *ApJ*, 449, L37
 Paczynski, B. 1986, *ApJ*, 308, L43
 Paczynski, B. 1998, *ApJ*, 494, L45
 Paczynski, B., & Rhoads, J.E. 1993, *ApJ*, 418, L5
 Pe'er, A., & Waxman, E. 2005, *ApJ*, in press (astro-ph/0409539)
 Panaitescu, A., & Meszaros, P. 1998 *ApJ*, 501, 702
 Pilla, R.P., & Loeb, A. 1998, *ApJ*, 494, L167
 Piran, T. 2000, *Phys. Rep.* 333, 529.
 Salmon, M.H., & Stecker, F.W. 1998, *ApJ*, 493, 547
 Sari, R., & Piran, T. 1995, *ApJ*, 455, L143
 Sari, R., & Piran, T. 1995, *ApJ*, 517, L109
 Sari, R., Piran, T., & Narayan, R. 1998, *ApJ*, 497, L17
 Schneid, E.J. et al. 1992, *A & A*, 255, L13
 Svensson, R. 1987, *MNRAS*, 227, 403
 Totani, T. 1998, *ApJ*, 502, L13
 Totani, T. 1998, *ApJ*, 509, L81
 Vietri, M. 1995, *ApJ*, 453, 883
 Vietri, M. 1997, *ApJ*, 478, L9
 Vietri, M. 1997, *Phys. Rev. Lett.*, 78, 4328
 Wang, X.Y., Dai, Z.G., & Lu, T. 2001, *ApJ*, 556, 1010
 Waxman, E. 1995a, *Phys. Rev. Lett.*, 75, 386
 Waxman, E. 1995b, *ApJ*, 452, L1
 Waxman, E. 1997, *ApJ*, 485, L5
 Waxman, E. 1997, *ApJ*, 489, L33
 Waxman, E. 1997, *ApJ*, 491, L19
 Waxman, E. 2003, in *Supernovae and Gamma-Ray Bursts*, Ed. K. Weiler (Springer), *Lecture Notes in Physics* 598, 393(418 (astro-ph/0303517)
 Waxman, E., & Bahcall, J. 1997, *Phys. Rev. Lett.*, 78, 2292
 Waxman, E., & Bahcall, J. 2000, *ApJ*, 541, 707
 Waxman, E., & Dainoff, B.T. 2000, *ApJ*, 537, 796
 Wei, D.M. 2003, *A & A*, 402, L9
 Willis, A.J. 1991, in *Wolf-Rayet Stars and Interrelations with other Massive stars in Galaxies*, ed. K.A. Van der Hucht & B. Heisterkamp (Dordrecht: Kluwer)
 Woosley, S.E. 1993, *ApJ*, 405, 273
 Zdziarski, A.A., & Lightman, A.P. 1985, *ApJ*, 294, L79
 Zhang, B., Kobayashi, S., & Meszaros, P. 2003, *ApJ*, 595, 950
 Zhang, B., & Meszaros, P. 2001, *ApJ*, 559, 110